Environ. Sci. Technol. **1998**, *32,* 2940−2946

Factors Influencing Photoreactions of Dissolved Organic Matter in a Coastal River of the Southeastern United States

HUIZHEN GAO

Oak Ridge Institute for Science and Education, Oak Ridge, Tennessee 37831

RICHARD G. ZEPP*

Ecosystems Research Division, National Exposure Research Laboratory, U.S. Environmental Protection Agency, Athens, Georgia 30605-2700

Photoreactions of dissolved organic matter can affect the oxidizing capacity, nutrient dynamics, trace gas exchange, and color of surface waters. This study focuses on factors that affect the photoreactions of the colored dissolved organic matter (CDOM) in the Satilla River, a coastal river that has high concentrations of dissolved organic carbon (DOC) (2.0 ± 0.2 mM C) and iron (12 ± 2 μM) in its freshwater reach. Quantum yields for the photoproduction of dissolved inorganic carbon (DIC) and carbon monoxide (CO) from Satilla CDOM decreased exponentially in the 300−450 nm spectral region. Photoreaction of the CDOM in sunlight caused a decrease in UV and visible absorbance that occurred most rapidly in the UV-B (280−315 nm) region, indicating that CDOM photoreactions can enhance exposure of aquatic organisms to DNA-damaging UV radiation. The role of iron in the photooxidation was investigated by adding fluoride ions or deferoxamine mesylate (DFOM) to the water to form unreactive Fe^{3+} complexes, thus inhibiting iron photoreduction and slowing CDOM photooxidation. Using this method, it was demonstrated that the photoformation of DIC, CO, and NH_4^+ is strongly affected by iron catalysis in the Satilla River water. Increasing the dioxygen content and lowering the pH accelerated the photoreaction of the CDOM. CDOM photoreaction was accompanied by conversion of dissolved iron and carbon to particulate forms. Such "photocoagulation" may contribute to the transport of iron and carbon from surface waters to sediments in sunlit, well-stratified aquatic ecosystems.

Introduction

The decomposition of nonliving terrestrial plant matter in part results in the production of colored polymers that are somewhat resistant to further microbial assimilation and breakdown. This colored organic matter, hydrophobic components of which have been referred to as "humic substances", occurs in soils (*1*) and also abounds in wetlands (*2*−*6*). When sunlight is absorbed by the colored dissolved organic matter (CDOM) in surface waters, a rich variety of photochemical reactions ensue. The resulting excited states of the CDOM and reactive transients produced therefrom participate in energy transfer, electron transfer, and free radical reactions that affect the fate of aquatic contaminants and the oxidizing capacity of the euphotic zone (*7*−*14*).

In addition to providing a primary source of reactive transients in aquatic environments, absorption of solar radiation by CDOM leads to its cleavage to a variety of photoproducts and to a reduction in its average molecular mass (*15*−*30*). These reactions include the direct photochemical mineralization of the CDOM to inorganic compounds, e.g., carbon monoxide, carbon dioxide, and other forms of dissolved inorganic carbon (DIC) (*24*−*26, 28, 29*).

Among other CDOM photoreactions are formation of nonvolatile carbon and nitrogen-containing compounds that are more biologically available than the unirradiated CDOM (*15, 20*−*23, 26*−*30*). These photoproducts absorb solar radiation more weakly than the unirradiated CDOM, and thus, CDOM photodegradation is accompanied by a reduction in the absorption coefficients of the DOM in the ultraviolet and visible spectral regions. Because CDOM is one of the most important sunlight-absorbing substances in freshwater and coastal environments, this reduction in absorbance, sometimes referred to as "photobleaching", can affect remote sensing of ocean color and permit deeper penetration of biologically effective UV-B radiation into the euphotic zone under stratified conditions (*31, 32*).

Several studies have indicated that the photodegradation of CDOM to DIC is catalyzed by iron (*11*−*14, 24, 34*−*38*). Stumm and Lee (*33*) demonstrated that iron can catalyze the oxidation of certain organic compounds by dioxygen. A subsequent study by Miles and Brezonik (*24*) demonstrated that irradiation by tungsten filament lamps enhanced dioxygen consumption and DIC production in aqueous solutions of humic substances that were spiked with iron (*24*). This catalysis involves oxidation of the DOM with concurrent reduction of Fe(III) to Fe(II), followed by reoxidation of the Fe(II) to Fe(III) by dioxygen and other oxidants [Fe(III) and Fe(II), respectively, refer to Fe^{3+} and Fe^{2+} and complexes thereof].

Since these pioneering studies, several other reports have appeared on the kinetics and mechanisms of the photooxidation of organic matter characteristic of aquatic environments (*9, 10, 15, 18, 19, 26, 30*), including the possible role of iron in these reactions (*9, 12*−*14, 34*−*37*). A schematic depicting some of the reactions that occur when CDOM is irradiated in water with dioxygen and iron present appears in Figure 1. Direct photolysis of CDOM produces a variety of photoproducts as well as reactive oxygen species that can participate in secondary reactions that transform the CDOM (*9, 18*). With iron present, light-induced reactions of CDOM can be accelerated by two general pathways: (1) direct photolysis of the Fe−CDOM carboxylate complexes via ligand-to-metal charge transfer, which results in formation of Fe(II) and polycarboxylate radicals that decarboxylate to form free radical intermediates; and (2) reactions between free radical intermediates and the Fe complexes that can further reduce the Fe(III) to Fe(II) and transform less reactive oxygen species such as superoxide into reactive oxidants such as hydroxyl radicals. Hydroxyl radicals are potent oxidants that could further oxidize the CDOM to DIC and other products. The diurnal variations in the concentration ratio of Fe(II) to Fe(III) that have been observed in field investigations of several freshwater systems (*12, 38*) indicate that sunlight plays an important role in iron redox reactions.

* Corresponding author phone: (706)355-8117; fax: (706)355-8104; e-mail: zepp.richard@epamail.epa.gov.

S0013-936X(98)00366-6 CCC: $15.00
Published on Web 08/12/1998

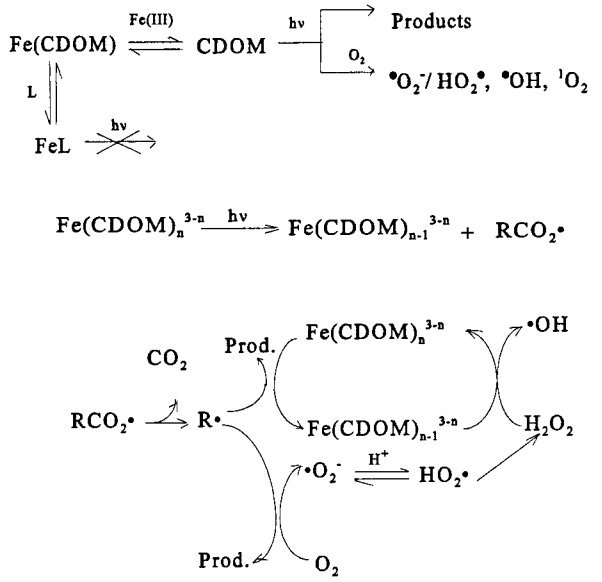

FIGURE 1. Scheme for the photooxidation reactions that occur in solutions of colored dissolved organic matter (CDOM) that contain iron and added ligands that react with Fe^{3+} to form non-photoreactive complexes.

We have conducted a study of the photochemical reactions of CDOM in filtered water recently obtained from the freshwater part of the Satilla River, which, like many coastal rivers with high DOC levels, is colored, acidic, and rich in iron. We present evidence that variations in wavelength, dioxygen concentration, and naturally occurring iron in the river water have important effects on the photokinetics of carbon gas formation, UV absorbance loss, and ammonium formation. Finally, we demonstrate that the CDOM photoreactions are accompanied by formation of particulate carbon and iron.

Experimental Section

Materials. Satilla River water (SRW) was collected at Atkinson, GA (81.86° W, 31.22° N). It was filtered immediately through 0.22 μm Millipore membrane filters and stored in the dark at 4 °C until it was used. All studies were conducted within 2 months of collection. After filtration, the samples of Satilla River water contained 2.0 ± 0.2 mM carbon and 12 ± 2 μM total dissolved iron. Recent data concerning the chemical composition of the Satilla River have been reported by Hopkinson et al. (39).

ACS-certified reagent-grade sodium fluoride (Matheson Coleman & Bell) and deferoxamine mesylate [1-amino-6,17-dihydroxy-7,10,18,21-tetraoxo-27-(*N*-acetylhydroxylamin)-6,11,17,22-tetraazoeicosane; also referred to as desferrioxamine B mesylate (DFOM)] (95% pure from Sigma) were used as received. CO standards were obtained from Scott-Marrin Corp. (500 ppb NIST traceable) and from the National Institute of Standards and Testing (20 ppm). The CO_2 standard (811 ppm) was obtained from Scott-Marrin. Reagent-grade potassium hydrogen phthalate and potassium ferrioxalate were obtained from Alfa. Other compounds were reagent-grade and were used as received. Water was treated with a Barnstead Nanopure model D-7331 purification system.

Fractionation of the DOM. The filtered SRW (8 L) was fractionated by a cross-flow ultrafiltration technique using membrane cassette filters (Pellicon2 cassette, Millipore Inc.). All membranes were extensively cleaned by flushing with purified water before they were used to avoid contamination; the cellulose acetate membrane (cutoff of 1 kDa) required extensive cleaning to reduce the DOC level of the permeate to <20 μM C. The SRW sample was initially pumped through a polyether sulfone membrane cassette filter (molecular mass cutoff of 10 kDa), and then the permeate of the 10 kDa membrane cassette was pumped through a cellulose membrane cassette with a molecular mass cutoff of 1 kDa. The retentate from the 10 kDa membrane cassette was defined as the fraction consisting mainly of dissolved organic matter (DOM) with a molecular mass of >10 kDa (MW > 10 kDa). The permeate from the 1 kDa membrane cassette was defined as the fraction consisting of DOM with a molecular mass <1 kDa (MW < 1 kDa). The retentate of the 1 kDa filter was defined as the fraction between 10 and 1 kDa (1 kDa < MW < 10 kDa). The >10 kDa fraction was not further concentrated. The remaining fractions were concentrated using a rotary evaporator. This procedure was repeated in triplicate. High recoveries (>90%) of the DOC and the iron were achieved with all three fractionations.

Equipment. Kinetic studies were carried out using a Suntest CPS solar simulator (Atlas Electric Devices) equipped with a xenon arc lamp and a Spectral Energy Monochromatic Illumination System which included a xenon arc lamp, grating monochromator, and sample compartment mounted on an optical bench. The spectral irradiance of the solar simulator in the UV region (295−400 nm, cutoff at 295 nm) was adjusted so that it closely matched that of midday solar spectral irradiance at Athens, GA (latitude of 34° N), on a clear June day.

Carbon monoxide and total carbon concentrations were measured using a Trace Analytical (Menlo Park, CA) RGA-3 Reduction Gas Analyzer. The data were acquired and analyzed by HP Chemstation software. Total carbon and DIC were measured using a Dohrmann DC-85A carbon analyzer (dioxygen as the carrier gas). In addition, DIC was measured in collaboration with W. Cai and Y. Wang (University of Georgia) by injecting sample aliquots into an acid bath (pH <2) and then purging the resulting CO_2 into a LICOR model 6252 infrared gas analyzer (IRGA). Electronic absorption spectra were obtained using a Shimadzu 265 spectrophotometer. For sample centrifugation, a Sorvall Superspeed (model RC-2, Ivan Sorvall Inc.) centrifuge was used.

Experimental Procedures. Water samples and the aqueous fractions were prepared for irradiation by bubbling for 30 min with either CO-free air (medical-grade), nitrogen (5.0-grade, trace oxygen removed by passage over a hot bed of copper catalyst), or dioxygen (4.4-grade). The pH was adjusted in some experiments by addition of dilute NaOH or HCl solutions. One set of samples was buffered with phosphate solution (pH 5.70, 5.0 mM). NaF or $NaClO_4$ (0.0010−0.2 M) and DFOM (0.133 mM) were added to the water for some of the studies. DIC and CO measurements were conducted as previously described (*26*) with the exception being that the kinetic effects of addition of Fe ligands on DIC production were investigated using the IRGA for CO_2 detection.

Ammonium concentrations were measured using a modified phenol/hypochlorite method (*40, 41*). The water samples were analyzed for nitrite and nitrate using a previously described absorptiometric procedure (*42*). The detection limit for this technique is 0.01 mg of N L^{-1} for nitrate and 5 μg of N L^{-1} for nitrite. Total iron was measured using a phenanthroline method (*42*). The Fe(II) also was determined using derivatization by phenanthroline; the absorbance of the Fe(II)−phenanthroline complex at 510 nm was determined within 5 min of the addition of the phenanthroline to the system. Control experiments showed that reduction of Fe(III) to Fe(II) by reducing constituents of the CDOM was negligible during this 5 min period.

The kinetic experiments in the solar simulator usually were conducted over a 72 h exposure period, with more

TABLE 1. Comparison of Kinetic Data for Formation and Loss of Selected Compounds on Exposure of Filtered Water Samples from the Satilla River to Simulated Solar Radiation[a,b]

compound or property	direction of concentration change (increase or decrease)	rate (M^{-1} h^{-1})	fractional conversion (h^{-1})
carbon dioxide	increase	2.2×10^{-5} [c]	1.0×10^{-2} [e]
carbon monoxide	increase	1.5×10^{-6} [c]	7.5×10^{-4} [e]
ammonium	increase	1.0×10^{-7} [c]	2.5×10^{-3} [f]
iron(II)	increase	9×10^{-5} [d]	7[g]
dioxygen	decrease	2.4×10^{-5} [c]	0.10[h]
UV-B absorption coefficient (300 nm)	decrease	not applicable	2.2×10^{-2} [i]

[a] Equivalent to mid-June sunlight, at a latitude of 34° N. [b] DOC was 2.1 mM with an absorption coefficient of 0.90 cm^{-1} at 350 nm; all solutions were air-saturated at 20 °C. [c] Average rate during the first 4 h of exposure. [d] Average rate during the first two min. [e] Conversion of TOC. [f] Conversion of dissolved organic nitrogen. [g] For approach to steady state [Fe(II)]. [h] Conversion of dioxygen. [i] Pseudo-first-order rate constant for photobleaching.

intensive sampling during the first 24 h period than in the remainder of the experiment. Shorter-term exposures were used for the studies of Fe(II) photoproduction. Dioxygen concentrations and pH were manipulated, and Fe(III) chelating ligands were added to determine the effects of iron on the photooxidation rates. Both fluoride and DFOM (0.10−0.13 mM), an excellent organic chelator of Fe(III) (*43*), were examined in the latter experiments.

The effects of centrifugation on the absorption spectra of the samples were conducted by spinning the samples of irradiated water at 10K rpm for 70 min. The relative centrifuge force was 2.96×10^4 dyn. After centrifugation, water was carefully removed from the upper 5.0 cm of the centrifuge tube. Under the conditions of this centrifugation, assuming that the density of the particles was 2.0 g/cm^3, the diameter of the particles that settled from this layer was computed to be >0.042 μm using the Stokes−Einstein equation.

Quantum yields for CO and DIC photoproduction were determined in triplicate using procedures that have been previously described (*25, 26*).

Results and Discussion

Photoproduct Kinetics. Irradiation of the Satilla River water samples and aqueous solutions of the fractionated DOM generally resulted in decreased absorbance in the UV and visible spectral region, i.e., photobleaching, that was accompanied by a decrease in DOC and dioxygen concentration and production of CO, DIC, and ammonium. The iron in the water samples was rapidly photoreduced to Fe(II), achieving a steady state within a few minutes. A comparison of the net rates of these various photoreactions in air-saturated river water with no manipulations of reaction conditions appears in Table 1.

As observed in other studies in natural waters, DIC was the most rapidly formed carbon-containing photoproduct, occurring about 15 times faster than CO formation (*26*). Ammonium, an important nutrient, was also produced by photodecomposition of the dissolved organic nitrogen, which was present at a concentration of 40 μM. Net nitrite and nitrate photoproduction were not detected using an absorptiometric method, even after irradiation for 72 h, indicating that their net formation rates were <5 nM h^{-1} for nitrite and <10 nM h^{-1} for nitrate, at least 1 order of magnitude slower than the ammonium formation rate. A low concentration of nitrate (~1−2 μM) was present in the SRW, and it slowly declined throughout the irradiation period. A number of carboxylic acids, other carbonyl-containing compounds, and volatile organic hydrocarbons (*46*) have been identified as photoproducts of CDOM (*15−23, 30, 46*). We observed a decrease in pH in the irradiated SRW that reflected the formation of such acidic products.

Photobleaching rate constants of the CDOM (Table 1 and Figure 2) are considerably larger than fractional conversion of TOC to DIC per unit time (Table 1). These results provide

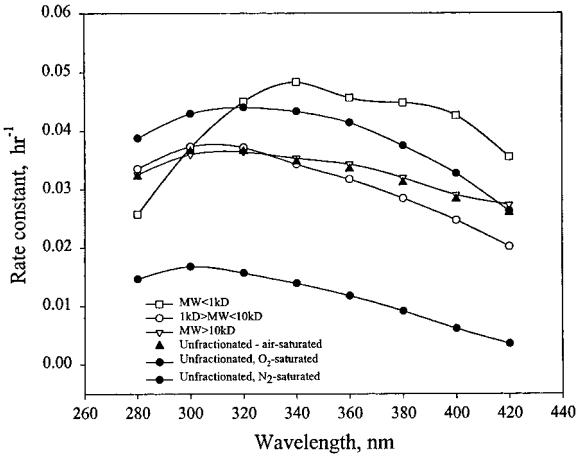

FIGURE 2. Pseudo-first-order rate constants for absorbance loss (photobleaching) in Satilla River water and in various fractions obtained by cross-flow ultrafiltration of the SRW. Effects of changing the dioxygen concentration on photobleaching kinetics of the SRW also are shown. Data are corrected for light attenuation effects (*26*).

further support to other findings (*26*) either that a large fraction of the photoreaction (at least 50%) must result in formation of yet-to-be-identified organic compounds that absorb much more weakly in the UV region than does the original CDOM or that a large fraction of the TOC in the original CDOM absorbs UV radiation very weakly. The results in Table 1 also show that the photooxidation of the CDOM results in net dioxygen consumption at a rate that is approximately the same as that of DIC formation. Most of the dioxygen consumed likely is converted to hydrogen peroxide; eventually, most of this peroxide is reoxidized to dioxygen or reduced to water (*9, 10, 13*).

Wavelength Dependence. Factors such as variations in the scalar irradiance caused by light attenuation and scattering in the water and variations in solar spectral irradiance can greatly alter the rates. To model these variations, quantum yields (or action spectra) are required (*30*). The wavelength dependence for CDOM photoreactions has been quantified through the determination of "action spectra", plots of the number of photoproduct molecules formed per incident photon versus wavelength. Action spectra can be constructed as plots of the cross product of absorption coefficient times the quantum yield (the number of molecules of photoproduct formed per photon absorbed) versus wavelength. Quantum yields provide a useful (unitless) yardstick for comparison of photoreactions of CDOM from different natural waters. Quantum yields for CO photoproduction in the Satilla River water (Table 2) were within a factor of 2−3 of those that have been previously observed in freshwaters (*25*), indicating that results from the Satilla River

TABLE 2. Quantum Yields, Absorption Coefficients, and Response Function for Photoproduction of Carbon Monoxide and Dissolved Inorganic Carbon from Satilla River Colored Dissolved Organic Matter

source	product	wavelength (nm)	$\phi_\lambda \times 10^5$	a_λ (cm^{-1})	$\phi_\lambda a_\lambda$ (cm^{-1})
unfractionated CDOM	DIC	290	8.0×10^2	2.188	1.75×10^{-2}
		350	2.0×10^2	0.940	1.88×10^{-3}
		390	32	0.336	1.1×10^{-4}
	CO	290	27	2.188	3.68×10^{-4}
		350	6.8	0.940	6.36×10^{-5}
		390	4.0	0.477	1.76×10^{-5}
		450	2.4	0.187	1.71×10^{-6}
MW > 10 kDa	DIC	290	9.3×10^2	1.847	1.72×10^{-2}
		350	2.9×10^2	0.811	2.3×10^{-3}
	CO	290	46.3	1.847	8.54×10^{-4}
		350	13.5	0.811	1.10×10^{-4}
		390	5.9	0.428	2.52×10^{-5}
		450	2.8	0.177	4.94×10^{-6}
1 kDa < MW < 10 kDa	DIC	290	8.25×10^2	1.294	1.07×10^{-2}
		350	2.45×10^2	0.479	1.2×10^{-3}
	CO	290	34.7	1.294	4.49×10^{-4}
		350	11.6	0.479	5.55×10^{-5}
		390	5.4	0.233	1.27×10^{-5}
		450	4.0	0.076	3.04×10^{-6}
MW < 1kDa	CO	290	69.7	0.424	2.95×10^{-4}
		350	20.7	0.131	2.72×10^{-5}

water are representative of other acidic waters with high CDOM concentrations.

The Satilla DOM was fractionated by cross-flow ultrafiltration into three fractions: MW > 10 kDa, 1 kDa < MW < 10 kDa, and MW < 1 kDa. These fractions accounted for 72, 25, and 2%, respectively, of the DOM mass. The membranes used for these separations were calibrated commercially using standards that have much different physicochemical properties than those of the anionic organic oligoelectrolytes that comprise CDOM. Factors such as ionic strength and pH are known to affect CDOM separations by ultrafiltration. Thus, the molecular mass ranges of CDOM fractions that are derived from these separations likely differ from those observed with the calibration standards. Nonetheless, several studies have demonstrated that ultrafiltration does separate natural colloids from coastal waters into fractions with differing chemical compositions, including differences in iron content (*47*). This was found to be the case with the Satilla River CDOM as well; almost all the color and iron was included in the MW > 10 kDa and 1 kDa < MW < 10 kDa fractions [Fe distribution, 2.5% in MW < 1 kDa, 21.1% in 1 kDa < MW < 10 kDa, and 76.3% in MW > 10 kDa; absorptivity at 440 nm [$(mM\ C)^{-1}\ cm^{-1}$], 0.0074 in MW < 1 kDa, 0.039 in 1 kDa < MW < 10 kDa, and 0.096 in MW > 10 kDa].

Quantum yields and absorption coefficients for the first two fractions were found to be similar to those of the unfractionated CDOM (Table 2). The quantum yields for the <1 kDa fraction were significantly higher than those for the other two. Fractions MW > 10 kDa and 1 kDa < MW < 10 kDa contained no detectable amounts of nitrate, a potential photochemical source of hydroxyl radicals, whereas the unfractionated water did contain a low concentration of nitrate ($\sim$2 μM). Thus, the results obtained with the unfractionated SRW were not significantly influenced by nitrate. Although the quantum yields for the MW < 1 kDa fraction were higher, it comprised such a small fraction of the CDOM that it made only a small contribution to the formation of CO and DIC from the unfractionated SRW. Quantum yields for DIC photoproduction were, as expected from the rates shown in Table 1, more than 1 order of magnitude higher than those for CO production.

Spectral Changes. CDOM photooxidation on exposure to simulated solar radiation also caused changes in the absorption spectrum of the CDOM. On continuous irradiation, the absorbance of the CDOM decreased throughout its UV and visible spectrum. Logarithmic plots of the absorption coefficients (2.303 times the absorbance ratioed to light path length) versus time were linear ($r^2 > 0.95$), at least through 75% loss of absorbance, indicating the bleaching could be described by a first-order rate expression. To compare the photobleaching kinetics of the unfractionated and fractionated CDOM, pseudo-first-order rate constants were computed for the bleaching at several wavelengths throughout the UV and visible region (Figure 2). The higher rate constants observed for bleaching of the <1 kDa fraction are consistent with the higher CO quantum yields for this fraction (Table 2). Moreover, the pseudo-first-order rate constants were wavelength-dependent, with the highest values in the UV-B region (280−315 nm) (Figure 2). This effect also was evident in the slope of exponential regressions of absorbance versus wavelength [previous studies have shown that the absorption spectra of CDOM exhibit exponential decreases in absorbance with increasing wavelength (*9, 10*)]. The slope S of logarithmic plots of absorbance versus wavelength decreased significantly as photooxidation proceeded (about 30% after exposure for 48 h). Similar observations have been reported for freshwater lakes in Pennsylvania (*32*). Consequently, exposure of CDOM to sunlight apparently results in a shift in the spectral distribution of the radiation that enhances the ratio of UV-B to UV-A radiation. This may be significant with respect to the ability of organisms to photorepair biological damage. Photorepair typically occurs most efficiently in the UV-A and short-wavelength visible region, whereas DNA damage occurs primarily on absorption of UV-B radiation.

Our conclusion that CDOM photooxidation leads to a decrease in S differs from that of Vodacek et al. (*31*). These investigators found that S increases along transects from the mouths of rivers out into the open ocean off the mid-Atlantic coast of the United States. This increase was attributed to photobleaching of the CDOM (*31*). We propose that these field observations can be explained by photobleaching in combination with a change in the source of the CDOM from decayed terrestrial plants to decomposed marine phytoplankton along the transects. However, depth-related changes in CDOM photoreaction rates (*30*), which shift the wavelength dependence more into the UV-A region (320−400 nm), might also be involved (*31*).

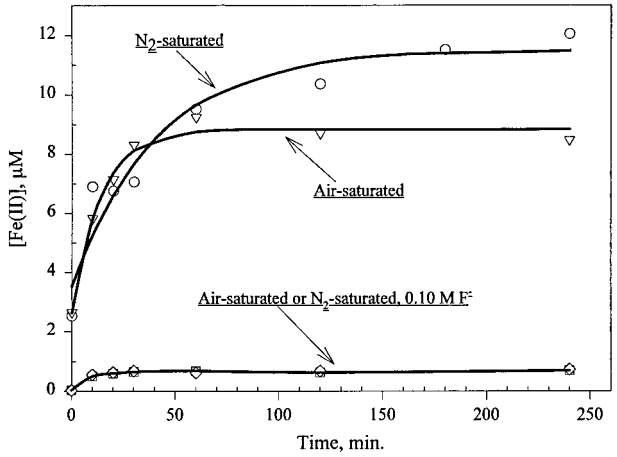

FIGURE 3. Photoreduction kinetics for naturally occurring iron in Satilla River water under various reaction conditions. Net photoreduction was strongly inhibited by addition of fluoride, a strong Fe^{3+} complexing ligand. Similar results were observed on addition of 0.13 M desferal. See Table 3 for more details about the composition of the solutions.

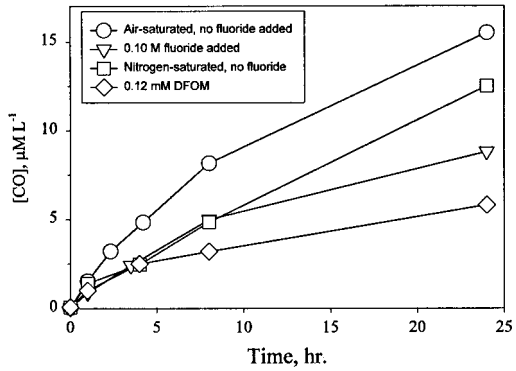

FIGURE 4. Photoproduction of carbon monoxide in Satilla River water under various reaction conditions. The initial rate (first 2 h) was the same in both air-saturated and nitrogen-saturated solutions, but the rate in the latter decreased with more prolonged irradiation. Complexation of the iron by fluoride and DFOM generally retarded CO photoproduction.

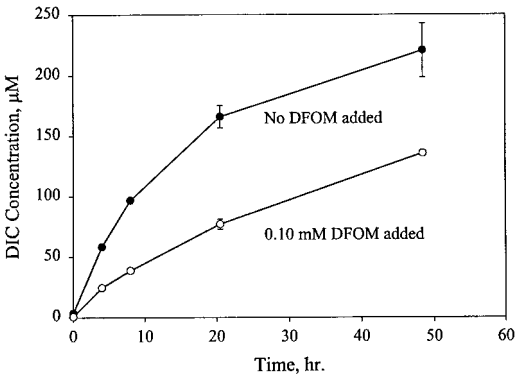

FIGURE 5. Effects of Fe^{3+} complexation by deferoxamine mesylate (DFOM) on the photoformation of DIC in Satilla River water.

Kinetic Effects of Dioxygen. Changes in dioxygen concentrations affected the photooxidation rates. As shown in Figure 2, increases in dioxygen concentration resulted in increases in the efficiency of photobleaching. Even under conditions in which dioxygen was carefully removed by extensive sparging with O_2-free nitrogen in a glovebox, photobleaching still occurred at a significant rate. Decreasing O_2 concentrations also decreased DIC formation rates. Fractional conversions of DOC to DIC (see the conditions in Table 1) were as follows: O_2-saturated, 0.012 h^{-1}; air-saturated, 0.010 h^{-1}; and N_2-saturated, 0.0040 h^{-1}. Dioxygen was consumed on irradiation of the CDOM, presumably via photoinduced electron (or hydrogen) transfer from CDOM (*9, 10, 48*). The effects of O_2 manipulations on CO photoproduction were more complex, with little apparent effect during the early stages of the photoreaction (first 2 h), even under nitrogen-saturated conditions, but pronounced decreases in the efficiency in N_2-saturated water after longer exposures. These results suggest that CO photoproduction occurs via at least two mechanisms: (1) dioxygen-independent direct photolysis of carbonyl precursors that are present in the CDOM at the start of irradiation and (2) direct photolysis of precursors that form via light-initiated autoxidation of the CDOM after irradiation is started. The latter source of precursors is dioxygen-dependent, so in the absence of dioxygen, the CO production rate is increasingly reduced with longer irradiation times as existing precursors are photodegraded.

Influence of Iron. To elucidate the influence of Fe on the kinetics of CDOM photooxidation, we added strong Fe(III) complexing ligands (symbolized by 'L' in Figure 1) to the water that formed nonphotoreactive (or at least inefficiently photoreactive) complexes. We chose fluoride and the siderophore DFOM (*43*) as the ligands. After addition of these ligands, the resulting solutions were not irradiated for at least 12 h to permit sufficient time for exchange of the Fe(III) from the CDOM ligands to the fluoride or DFOM ligands. Complexation of Fe(III) by fluoride, a poor electron-accepting ligand that has no ligand-to-metal charge transfer absorption, virtually eliminates Fe-related absorption at wavelengths of >260 nm. Hence, the fluoride complex does not photoreact when it is exposed to solar radiation, which effectively cuts off at wavelengths of >295 nm. A control study of the spectral properties and direct photolysis of the Fe^{3+}−DFOM complex (15 μM Fe and 100 μM DFOM) in deionized water indicated that (a) the complex does not absorb light significantly at wavelengths of >295 nm, the cutoff for solar radiation, and (b) not surprisingly, no photoreduction to Fe(II) or changes in the UV spectrum occurred over a 24 h/period of irradiation in the solar simulator. Fluoride ions had the advantage (over DFOM) in that they are virtually inert to attack by the reactive oxygen species that mediate CDOM photoreactions. Thus, most of our studies of Fe involvement were conducted using fluoride as the ligand.

That fluoride (0.10 M) extensively complexed the Fe(III) was evidenced by a sharp reduction in the photoreduction rate of Fe(III) to Fe(II) with fluoride present (Figure 3). This reduction was unchanged in anaerobic (N_2-saturated) water, indicating that the effect could not be attributed to enhanced oxidation of Fe(II) to Fe(III) in the presence of this ligand. Even at much lower fluoride concentrations (0.0010 M), initial Fe(II) photoproduction in air-saturated Satilla River water was slowed to less than 20% of that when no fluoride was added. Similar results were obtained with 0.13 mM DFOM present; no increase in Fe(II) concentration occurred after irradiation for up to 8.0 h in the solar simulator.

The effects of Fe^{3+} complexation by added fluoride or DFOM on the CDOM photooxidation kinetics were pronounced (Figures 4 and 5 and Table 3). Addition of fluoride (0.001−0.10 M) and DFOM (0.12 mM) attenuated the photoproduction of CO and DIC. In the case of CO (Figure 4), this effect must result from the lower photoproduction rate of reactive oxygen species when iron complexation to CDOM is reduced. The addition of DFOM (0.13 mM) decreased the photoproduction rate of CO to a greater extent than did fluoride (0.10 M). This result indicates that DFOM, in addition to inhibiting Fe catalysis, also may be scavenging

TABLE 3. Effect of Added Fe Ligands, Fluoride and Deferoxamine Mesylate (DFOM), on the Photoproduction of DIC and CO from Satilla River CDOM[a,b]

added ligand	CO_2 rate (M^{-1} h^{-1})[c]	CO rate (M^{-1} h^{-1})[c]
no ligand added	2.2×10^{-5}	1.5×10^{-6}
0.10 M F^-	1.6×10^{-5}	1.3×10^{-6}
0.050 M F^-	1.4×10^{-5}	1.4×10^{-6}
0.0010 M F^-	1.7×10^{-5}	1.3×10^{-6}
0.00013 M DFOM	1.0×10^{-5}	1.1×10^{-6}

[a] Data are normalized to the water sample with an absorption coefficient of 0.90 cm^{-1} at 350 nm. [b] See Table 1 for reaction conditions. [c] Average rate during the first 24 h of exposure, corrected for light attenuation effects; the standard deviation of rate constants was ±15% of the average.

reactive oxidizing species that are involved in CO production, e.g., inhibiting formation of CO precursors.

DIC photoformation also was slowed on addition of DFOM and fluoride (Figure 5 and Table 3). Fluoride concentrations were varied in the Satilla River water to learn more about the quantitative role of Fe photoreactions in CDOM photooxidation. As shown in Table 3, fluoride significantly slowed DIC photoformation at fluoride concentrations as low as 0.0010 mM. Increasing the fluoride concentration by 2 orders of magnitude (from 0.0010 to 0.10 M) had comparatively minor effects on DIC photoproduction (Table 3). These results were similar to those observed in the case of fluoride effects on iron photoreduction where a major rate reduction was observed at 0.0010 mM and relatively minor changes in rate were measured on increasing the fluoride concentration to 0.10 M. Similar trends were observed in the case of CO photoproduction, although the rates were not as responsive to addition of fluoride (Table 3).

The effect of added fluoride on CDOM photooxidation was pH-dependent. Increasing the pH from 4.0 to 7.0 significantly increased the rate of DIC formation in the absence of fluoride (from 20 μmol h^{-1} at pH 4.0 to 30 μmol h^{-1} at pH 7.0), but the rate was reduced and the pH effect was eliminated when fluoride (0.10 M) was present (15 μmol h^{-1} at both pH 4.0 and 7.0). In a previous study of DIC formation in water samples collected in coastal regions, little pH effect on photochemical DIC formation was observed, possibly reflecting a lack of reactive iron in the water (*26*).

Other effects of fluoride were observed. (1) As previously reported for water samples from other freshwaters (*27*), we found that acidification from pH 7.0 to 4.0 increased the rate of photochemical ammonium production from 0.036 to 0.056 μmol h^{-1}, a 55% increase. Addition of fluoride (0.10 M) attenuated this photoammonification to 0.026 μmol h^{-1} at pH 7.0 and 0.033 μmol h^{-1} at pH 4.0. (2) The complexation of Fe by fluoride also affected the photooxidation of CDOM to acidic photoproducts. The reduction of pH during a 4.0 h period of irradiation was less (0.28 unit) with fluoride added than in the original SRW (0.51 unit), indicating that organic acid production is reduced.

These results clearly demonstrate that naturally occurring iron can catalyze the photooxidation of CDOM in high-DOC freshwaters. Another important finding of these studies is that, even under conditions in which the Fe(III) was quantitatively complexed, photooxidation to DIC, CO, and NH_4^+ still occurred at an environmentally significant rate (Table 3). In the case of CDOM photobleaching, little or no effect of added fluoride or DFOM was observed. This indicates that a major part of the CDOM photoreaction in this iron-rich river water does not involve the participation of iron. Other reaction pathways involving direct photoreactions of the CDOM and secondary reactions involving reactive oxygen species are involved in iron-independent photooxidation (Figure 1).

Photooxidation and DOM Coagulation. A variety of processes can affect the kinetics and extent of DOM coagulation (*49*). The possible influence of photooxidation has not been widely discussed. We observed, however, that the photobleaching in the O_2-saturated SRW was accompanied by visible brown precipitation after irradiation for 72 h.

Particulate formation was demonstrated by examining the effects of high-speed centrifugation on the absorption spectrum and composition of air-saturated and dioxygen-saturated irradiated water samples. The UV−visible attenuation of the centrifuged samples, especially for the O_2-saturated sample, was reduced compared to that before centrifugation, indicating that colloidal particles in the water were substantially contributing to light attenuation by scattering and absorption. The diameter of the particles remaining in the centrifuged water was estimated to be <0.042 μm on the basis of calculations using the Stokes−Einstein equation. Centrifugation of a dark control (0.2 μm filtered SRW) resulted in no detectable change in its absorption spectrum.

Additional studies were conducted to better understand the nature of the particles that were produced. Comparison of the iron and DOC concentrations in the irradiated SRW (irradiation for 72 h) and in the supernatant of the centrifuged, irradiated SRW showed that centrifugation reduced total iron from 10 to 5.5 μM and DOC from 11.2 to 9.7 mg of C L^{-1}. These results indicate that photooxidation of the CDOM in the Satilla River water results in substantial conversion of the iron to particles, probably polymeric iron oxides, and in some conversion of the DOC to particulate organic carbon (POC).

Extensive photooxidation undoubtedly must alter diffuse double-layer repulsion and van der Waals attraction between the organic colloids that comprise CDOM (*49*). The formation of DIC indicates, for example, that carboxylate moieties are being oxidized, a process that must alter these factors. Moreover, as the CDOM oxidizes, so must its ability to complex iron; Fe(III) thus must more extensively hydrolyze to hydroxy complexes which then form polymeric iron oxides. The iron oxides in turn may induce further aggregation of the CDOM.

Thus, CDOM photooxidation may contribute to the coagulation of DOM in aquatic environments. This process is likely to be of greatest importance in stratified waters that are exposed to high levels of solar UV radiation, e.g., lakes and estuaries during the summer in temperate regions and year-round in the tropics and subtropics.

Acknowledgments

This paper is dedicated to Professor Werner Stumm, whose pioneering studies of iron redox reactions with natural organic matter provided the conceptual basis for much of the research described herein. This project was conducted as part of the Georgia Rivers Land Margin Ecosystem Research (LMER) project. We thank M. Moran and other scientists involved in this project for providing access to LMER sampling sites on the Satilla River, for assisting with periodic collection of water samples, for providing ancillary data concerning environmental conditions at the sites, and for providing prepublications of their research at the sites. We express appreciation to W. Cai and Y. Wang for assisting with DIC measurements and to W. Sunda for helpful discussions concerning iron complexation. H.G. thanks the Oak Ridge Institute for Science and Education for financial support. R.Z. acknowledges support from EPA Internal Grant AT01E5.

Supporting Information Available

Four figures depicting results of different experiments carried out with Satilla River water (4 pages). Ordering information is given on any current masthead page.

Literature Cited

(1) Stevenson, F. J. *Humus Chemistry*; Wiley: New York, 1994.
(2) Thurman, E. M. *Organic Geochemistry of Natural Waters*; Nijhoff/Junk: Boston, 1985; 497 pp.
(3) Aiken, G. R., McKnight, D. M., Wershaw, R. L., MacCarthy, P., Eds. *Humic Substances in Soil, Sediment and Water: Geochemistry, Isolation and Characterization*; Wiley-Interscience: New York, 1985; 691 pp.
(4) Wetzel, R. G. *Hydrobiologia* **1992**, *229*, 181−198.
(5) Moran, M. A.; Hodson, R. E. *Limnol. Oceanogr.* **1994**, *39*, 762−771.
(6) Opsahl, S.; Benner, R. *Nature* **1997**, *386*, 480−482.
(7) Zafiriou, O. C.; Joussot-Dubien, J.; Zepp, R. G.; Zika, R. G. *Environ. Sci. Technol.* **1984**, *18*, 358A−371A.
(8) Hoigné, J.; Faust, B. C.; Haag, W. R.; Scully, F. E., Jr.; Zepp, R. G. In *Advances in Chemistry Series No. 219, Aquatic Humic Substances: Influence on Fate and Treatment of Pollutants*; Suffit, I. H., MacCarthy, P., Eds.; American Chemical Society: Washington, DC, 1989; p 363.
(9) Blough, N. V.; Zepp, R. G. In *Active Oxygen: Reactive Oxygen Species in Chemistry*; Foote, C. S., Valentine, J., Eds.; Chapman and Hall: New York, 1995; pp 280−333.
(10) Blough, N. V. In *The Sea Surface and Global Change*; Duce, R., Liss, P., Duce, R., Eds.; Cambridge University Press: Cambridge, U.K., 1996.
(11) Stumm, W.; Sulzberger, B. *Geochim. Cosmochim. Acta* **1991**, *56*, 3233−3257.
(12) Faust, B. C. In *Aquatic and Surface Photochemistry*; Helz, G. R., Zepp, R. G., Crosby, D. G., Eds.; Lewis Publishers: Ann Arbor, MI, 1994; pp 3−39.
(13) (a) Voelker, B. M.; Sulzberger, B. *Environ. Sci. Technol.* **1996**, *30*, 1106−1114. (b)Voelker, B.; Morel, F. M. M.; Sulzberger, B. *Environ. Sci. Technol.* **1997**, *31*, 1004−1011.
(14) Waite, T. D.; Szymczak, R. In *Aquatic and Surface Photochemistry*; Helz, G. R., Zepp, R. G., Crosby, D. G., Eds.; Lewis Publishers: Ann Arbor, MI, 1994; pp 39−53.
(15) Kieber, D. J.; McDaniel, J.; Mopper, K. *Nature* **1989**, *341*, 637−639.
(16) Kieber, D. J.; Mopper, K. *Mar. Chem.* **1987**, *21*, 135−149.
(17) Kieber, R. J.; Zhou, X.; Mopper, K. *Limnol. Oceanogr.* **1990**, *35*, 1503−1515.
(18) Mopper, K.; Zhou, X. *Science* **1990**, *250*, 661−664.
(19) Mopper, K.; Zhou, X.; Kieber, R. J.; Kieber, D. J.; Sikorski, R. J.; Jones, R. D. *Nature* **1991**, *353*, 60−62.
(20) Wetzel, R. G.; Hatcher, P. G.; Bianchi, T. S. *Limnol. Oceanogr.* **1995**, *40*, 1369−1380.
(21) Amador, J. A.; Alexander, M.; Zika, R. G. *Appl. Environ. Microbiol.* **1989**, *55*, 2843−2849.
(22) De Haan, H. *Limnol. Oceanogr.* **1993**, *38*, 1072−1076.
(23) Hongve, D. *Acta Hydrochim. Hydrobiol.* **1994**, *3*, 117−120.
(24) Miles, C. J.; Brezonik, P. L. *Environ. Sci. Technol.* **1981**, *15*, 1089−1095.
(25) Valentine, R. L.; Zepp, R. G. *Environ. Sci. Technol.* **1993**, *27*, 409−412.
(26) Miller, W. L.; Zepp, R. G. *Geophys. Res. Lett.* **1995**, *22*, 417−420.
(27) Bushaw, K. L.; Zepp, R. G.; Tarr, M. A.; Schulz-Jander, D.; Bourbonniere, R. A.; Hodson, R. E.; Miller, W. L.; Bronk, D. A.; Moran, M. A. *Nature* **1996**, *381*, 404−407.
(28) Amon, R. M. W.; Benner, R. *Geochim. Cosmochim. Acta* **1996**, *60*, 1783−1792.
(29) Granéli, W.; Lindell, M.; Tranvik, L. *Limnol. Oceanogr.* **1996**, *41*, 698−706.
(30) Moran, M. A.; Zepp, R. G. *Limnol. Oceanogr.* **1987**, *42*, 1307−1316.
(31) Vodacek, A.; Degrandpre, M. D.; Peltzer, E. D.; Nelson, R. K.; Blough, N. V. *Limnol. Oceanogr.* **1997**, *42*, 674−686.
(32) Morris, D. P.; Hargreaves, B. R. *Limnol. Oceanogr.* **1997**, *42*, 239−249.
(33) Stumm, W.; Lee, G. F. *Ind. Eng. Chem.* **1961**, *53*, 143−146.
(34) Faust, B. C.; Zepp, R. G. *Environ. Sci. Technol.* **1993**, *27*, 2517−2522.
(35) Zuo, Y.; Hoigné, J. *Environ. Sci. Technol.* **1992**, *26*, 1014−1022.
(36) Voelker, B.; Sedlak, D. L. *Mar. Chem.* **1995**, *50*, 93−102.
(37) Zepp, R. G.; Faust, B. C.; Hoigné, J. *Environ. Sci. Technol.* **1992**, *26*, 313−319.
(38) McKnight, D. M.; Kimball, B. A.; Bencala, K. E. *Science* **1988**, *240*, 637−640.
(39) Hopkinson, C. S.; Fry, B.; Nolin, A. L. *Cont. Shelf Res.* **1997**, *17*, 473−489.
(40) Grasshoff, K., Ehrhardt, M., Kremling, K., Eds. *Methods of Seawater Analysis*; Verlag Chemie: Weinheim, Germany, 1983.
(41) Strickland, J. D.; Parsons, T. R. *A Practical Handbook of Seawater Analysis*; Canadian Government Publish Center, Supply and Services Canada: Ottawa, Canada, 1972.
(42) *Standard Methods for the Examination of Water and Wastewater*, 18th ed.; APHA, AWWA, and WEF: Washington, DC, 1992.
(43) Hudson, R. J. M.; Covault, D. T.; Morel, F. M. M. *Mar. Chem.* **1992**, *38*, 209−235.
(44) Bushaw, K. L. Ph.D. Dissertation, University of Georgia, Athens, GA, 1997.
(45) Miller, W. L.; Moran, M. A. *Limnol. Oceanogr.* **1997**, *42*, 1317−1324.
(46) Reimer, D. D.; Pos, W. H.; Milne, P. J.; Zika, R. G. *J. Geophys. Res., Atmos.* Submitted for publication.
(47) Powell, R. T.; Landing, W. M.; Bauer, J. E. *Mar. Chem.* **1996**, *55*, 165−176.
(48) Zepp, R. G.; Braun, A. M.; Hoigné, J.; Leenheer, J. A. *Environ. Sci. Technol.* **1987**, *21*, 485−490.
(49) Stumm, W.; Morgan, J. J. *Aquatic Chemistry*, 3rd ed.; Wiley: New York, 1996; pp 818−871.

Received for review April 13, 1998. Revised manuscript received June 1, 1998. Accepted June 15, 1998.

ES9803660